eNeuro

Research Article: Methods/New Tools | Novel Tools and Methods

3DMorph automatic analysis of microglial morphology in 3 dimensions from *ex vivo* and *in vivo* imaging

Elisa M. York[1], Jeffrey M. LeDue[1], Louis-Philippe Bernier[1] and Brian A. MacVicar[1]

[1]*Department of Psychiatry, Djavad Mowafaghian Centre for Brain Health, University of British Columbia, British Columbia, V6T 1Z3, Canada*

https://doi.org/10.1523/ENEURO.0266-18.2018

Received: 9 July 2018

Revised: 18 October 2018

Accepted: 28 October 2018

Published: 19 November 2018

Author Contributions: EMY and JML designed research and performed research; LPB analyzed data and contributed unpublished analytical tools; EMY wrote the paper; All authors contributed to editing the paper and giving feedback during the code development process.

Funding: http://doi.org/10.13039/501100000024Gouvernement du Canada | Canadian Institutes of Health Research (CIHR)
148397

Funding: Foundation Leducq

Conflict of Interest: No contributing authors have any conflicts of interest to declare.

A Canada Research Chair in Neuroscience to B.A.M., a Foundation grant (#148397) from Canadian Institutes of Health Research, and a grant from Fondation Leducq to B.A.M.

Correspondence should be addressed to Elisa M. York, Djavad Mowafaghian Centre for Brain Health, 2215 Wesbrook Mall, Vancouver, BC Canada, V6T 1Z3. E-mail: elisa.york@alumni.ubc.ca, or Brain A. MacVicar, Djavad Mowafaghian Centre for Brain Health, 2215 Wesbrook Mall, Vancouver, BC Canada, V6T 1Z3. E-mail: bmacvicar@brain.ubc.ca.

Cite as: eNeuro 2018; 10.1523/ENEURO.0266-18.2018

Title

3DMorph automatic analysis of microglial morphology in 3 dimensions from *ex vivo* and *in vivo* imaging

Abbreviated Title

3DMorph analysis of microglial morphology

Author Names

Elisa M. York[1], Jeffrey M. LeDue[1], Louis-Philippe Bernier[1], Brian A. MacVicar[1]

Affiliations

[1] Department of Psychiatry, Djavad Mowafaghian Centre for Brain Health, University of British Columbia, British Columbia, Canada, V6T 1Z3

Author Contributions

EMY and JML designed research and performed research; LPB analyzed data and contributed unpublished analytical tools; EMY wrote the paper; All authors contributed to editing the paper and giving feedback during the code development process.

Correspondence should be addressed to

1. Elisa M. York, elisa.york@alumni.ubc.ca
Djavad Mowafaghian Centre for Brain Health
2215 Wesbrook Mall
Vancouver, BC Canada
V6T 1Z3

2. Dr. Brain A. MacVicar, bmacvicar@brain.ubc.ca
Djavad Mowafaghian Centre for Brain Health
2215 Wesbrook Mall
Vancouver, BC Canada
V6T 1Z3

Number of Figures: 7

Number of Tables: 1

Number of Multimedia: 0

Number of Words in Abstract: 236

Number of Significance Statement: 120

Number of Words in Introduction: 482

Number of Words in Discussion: 1077

Acknowledgments

The authors would like to thank Dr. Lasse Dissing-Olesen (Department of Neurology, F.M. Kirby Neurobiology Center, Boston Children's Hospital, Harvard Medical School, Boston, USA) and Dr. Jasmin K. Hefendehl (Department of Cellular Neurology, Hertie Institute for Clinical Brain Research, University of Tübingen, Tübingen, Germany) for the gracious use of the *in vivo* images for processing by 3DMorph, and for their valuable comments on the manuscript. The authors also thank Dr. Nick L. Weilinger (Department of Psychiatry, Djavad Mowafaghian Centre for Brain Health, University of British Columbia, British Columbia, Canada) for patching and imaging neurons for processing by 3DMorph, and for providing constructive feedback on the manuscript. Finally, we thank the Canadian Institutes of Health Research and Fondation Leducq for their generous funding support.

Conflicts of Interest

No contributing authors have any conflicts of interest to declare.

Funding Sources

47 A Canada Research Chair in Neuroscience to B.A.M., a Foundation grant (#148397) from Canadian

48 Institutes of Health Research, and a grant from Fondation Leducq to B.A.M

49

3

Abstract

Microglia are dynamic immune cells of the central nervous system, and their morphology is commonly used as a readout of cellular function. However, current morphological analysis techniques rely on either tracing of cells or 2D projection analysis, which are time-consuming, subject to bias, and may ignore important three-dimensional (3D) information. Therefore, we have created 3DMorph, a Matlab-based script that analyzes microglial morphology from 3D data. The program initially requires input of threshold levels, cell size expectations, and preferred methods of skeletonization. This makes 3DMorph easily scalable and adaptable to different imaging parameters or cell types. After these settings are defined, the program is completely automatic and can batch process files without user input. Output data includes cell volume, territorial volume, branch length, number of endpoints and branch points, and average distance between cells. We show that 3DMorph is accurate when compared to manual tracing, with significantly decreased user input time. Importantly, 3DMorph is capable of processing *in vivo* microglial morphology, as well as other 3D branching cell types, from mouse cranial windows or acute hippocampal slices. Therefore, we present a novel, user-friendly, scalable, and semi-automatic method of analyzing cell morphology in 3 dimensions. This method should improve the accuracy of cell measurements, remove user bias between conditions, increase reproducibility between experimenters and labs, and reduce user input time. We provide this open source code on GitHub so that it is free and accessible to all investigators.

4

74

75 **Significance Statement**

76 Microglial morphology is often considered to be an indicator of cellular activity, however current
77 techniques to analyze morphology either lose valuable z-dimension information or are time intensive to
78 perform. Therefore, we introduce 3DMorph, a MATLAB-based program that semi-automatically
79 processes individual microglial morphology from overlapping 3D clusters, improving accuracy and
80 processing time compared to current tools. 3DMorph is straightforward to use and adaptable to many
81 imaging or experimental parameters. Once user settings are selected, 3DMorph can run in batch mode
82 to automatically process multiple files. We validate 3DMorph against current techniques, and
83 demonstrate the ability to detect differences in microglial morphologies from different *ex vivo*
84 experimental conditions, as well as from *in vivo* data, and images of other branching cell types.

85

86

5

Introduction

Microglia, the immune cells of the central nervous system, have small cell bodies and ramified processes that survey the local environment for signs of infection, damage, or disruption of molecular homeostasis (Nimmerjahn, Kirchhoff, & Helmchen, 2005). In response to sensing damage, microglia rapidly extend their processes to converge at the site of injury (Davalos et al., 2005; Dissing-Olesen et al., 2014; Drew et al., 2010; Eyo et al., 2014, 2015; Hines, Hines, Mulligan, & Macvicar, 2009; Lou et al., 2016; Nimmerjahn et al., 2005). Upon extensive damage of surrounding cells or stimulation by pathogen-associated triggers, microglia retract their processes to adopt an amoeboid morphology (Doorn et al., 2014; Kloss, Bohatschek, Kreutzberg, & Raivich, 2001; Kreutzberg, 1996).

As a result of these contextual morphological changes, microglial shape and process ramification have been used as correlates of cellular function (Davis, Foster, & Thomas, 1994; Karperien, Ahammer, & Jelinek, 2013), with several methods developed to quantify their morphology. Current approaches include manually tracing processes throughout z-stack images (Baron, Babcock, Nemirovsky, Finsen, & Monsonego, 2014; Takayama, Hayashi, Wu, Liu, & Nakanishi, 2016), or performing morphological analysis on a 2-dimensional maximum projection (Karperien et al., 2013; Kozlowski & Weimer, 2012; Torres-Platas et al., 2014; Verdonk et al., 2016). The first method is time-intensive and subject to experimenter bias and variability. The second technique loses 3D information, leading to underestimation of process lengths or erroneous connection of processes. Three dimensional reconstructions of microglia cells can be generated using software such as Imaris (Erny et al., 2015; Perego, Fumagalli, & De Simoni, 2013); however, this is time-intensive and expensive. There is a clear need for a method that performs unbiased and automatic analysis of the 3D microglial structure observed in *ex vivo* and *in vivo* systems.

6

Here, we describe a method for semi-automatic analysis of microglial morphology in 3D using a custom Matlab script, 3DMorph. The program uses graphical user interfaces to initially define image threshold, noise limits, and cell sizes. Once these settings are selected, a parameters file is saved that can be used to automatically batch process multiple files. From each image, an Excel file is saved with output data from the entire image (volume covered, average centroid distance), as well as from individual cells within the image (territorial volume, cell volume, cell ramification index, number of endpoints and branch points, and average, min, and max branch lengths).

The utility of 3DMorph is validated by analyzing and quantifying typical examples of morphological changes of groups of microglia under control conditions, after hyper-ramification triggered by ATP application, and after retraction of ramifications triggered by inhibiting neuronal AMPA receptors with CNQX and action potentials with TTX. 3DMorph is also shown to process *in vivo* microglial images, as well as other branching cell types such as neurons. Therefore, this analysis software will allow for the automatic and unbiased analysis of microglial morphologies in 3D under several experimental and pathological conditions.

Materials and Methods

Animal Protocols

All housing and experimental procedures were carried out in accordance with University of British Columbia and Canadian Council on Animal Care regulations. CX3CR1$^{EGFP/EGFP}$ or CX3CR1$^{+/EGFP}$ mice on a C57Bl/6 background (Jung et al., 2000) were housed in a 12 h light/day cycle with food and water *ad libitum*.

7

Acute Hippocampal Slice Preparation

Male mice (2 months of age) were anesthetized to surgical plane with isoflurane and decapitated according to protocols approved by the University of British Columbia committee on animal care. Brains were dissected and sliced horizontally with a vibratome (Leica VT1200S) at 300 µm thick in ice-cold NMDG slicing solution containing (in mM): 120 N-methyl-D-glucamine, 2.5 KCl, 25 $NaHCO_3$, 1 $CaCl_2$, 7 $MgCl_2$, 1.2 NaH_2PO_4, 2 D-glucose, 2.4 sodium pyruvate, and 1.3 sodium L-ascorbate, which was constantly oxygenated with 95% O_2 and 5% CO_2. Hippocampal slices were immediately transferred to artificial cerebral spinal fluid (aCSF) continuously oxygenated with 95% O_2 and 5% CO_2, and allowed to recover for 30 minutes at 32 ˚C. Artificial CSF contained (in mM): 126 NaCl, 2.5 KCl, 26 $NaHCO_3$, 2 $CaCl_2$, 2 $MgCl_2$, 1.25 NaH_2PO_4, and 10 D-glucose, pH 7.3–7.4, osmolarity 300 mOsm.

Treatment Conditions and SNAPSHOT

Slices were incubated for 10 min at 32 °C in either control aCSF, or aCSF containing 500 µM ATP, or 50 µM CNQX and 1 µM TTX. Slices were then fixed using the SNAPSHOT method (Dissing-Olesen & MacVicar, 2015), which consists of a 2 minute immersion in 4% PFA at 80 ˚C, rinse in 0.1 M PBS, and storage in clearing solution (0.1M PBS with 20% DMSO, and 2% triton X) at 4 ˚C for one week. GFP fluorescence is well-preserved by this method, and slices were ready for imaging immediately after clearing.

Acute Hippocampal Slice Image Acquisition

Fixed hippocampal slices were imaged with a two-photon Coherent Chameleon Ultra II laser with a Zeiss LSM 7 MP microscope. Using a Zeiss 20x-W/1.0 NA objective, GFP was excited at 920 nm, and emission was detected by a photo-multiplier tube (Zeiss LSM BiG) after passing through a 535 ± 25 nm filter. Images were taken in the stratum radiatum of CA1 hippocampus at a depth of 150 µm ± 25 µm. Stacks were imaged at 16-bit, with 1024 x 1024 pixels, 16-line averaging, a zoom of 2.8, and z-step distance of 1

8

152 µm. After acquisition, background signal was removed from all images using Fiji's rolling ball (radius = 25
153 pixels) background subtraction.

154 Cranial Window Surgery

155 Mice were anesthetized using a tricomponent anesthesia (fentanyl, 0.05 mg/kg; midazolam, 5 mg/kg;
156 medetomidine, 0.50 mg/kg), placed on a heating pad, and secured to a stereotactic frame. After the
157 skull was exposed by removing the skin and periosteum, a circle was gently drilled into the skull's
158 surface at 0.5 mm lateral of -0.5 mm bregma. Once this portion of skull was removed, the brain was kept
159 moist using surgical gel sponges in PBS (GelitaSpon). A custom-made 14 mm diameter titanium ring was
160 secured around the cranial window with light-curing dental cement (Heraeus). This ring fits into a
161 custom-made head fixation plate, which secures the skull in the x, y, and z planes during *in vivo* imaging
162 (Hefendehl et al., 2014).

163 *In Vivo* Image Acquisition

164 After cranial window preparation and titanium head ring fixation, anesthetized mice (fentanyl, 0.05
165 mg/kg; midazolam, 5 mg/kg; medetomidine, 0.50 mg/kg) were imaged on a custom-made two-photon
166 microscope (Rosenegger, Tran, LeDue, Zhou, & Gordon, 2014) using a Coherent Chameleon Ultra II laser
167 and a Zeiss 40X-W/1 NA objective. The head ring is secured to a fixation plate (Hefendehl et al., 2014),
168 which is connected to a motorized x-y stage (Sutter Instruments). EGFP was imaged with 920 nm
169 excitation and detected via non-descanned detectors after passing an ET525/50m-2P emission filter
170 (Chroma Technology). Laser power did not exceed 45 mW throughout the experiment. Z-stack images (z
171 = 40; 1 µm steps) were acquired at 512 x 512 pixels with no averaging, at a depth of 100 - 140 µm. Using
172 a custom-designed perfusion system, aCSF was continuously perfused across the cortical surface at a
173 rate of 3 ml/min. After acquisition, the signal of EGFP in these images was enhanced by increasing the
174 contrast in Fiji, and motion artifacts were corrected with the Gaussian 3D filter.

Neuronal Dye Loading

Layer 3 neurons from acute cortical slices (P24 rat) were whole-cell patch clamped with borosilicate glass electrodes (3-4 MΩ). The intracellular recording solution consisted of (in mM): 113 K-gluconate, 2 $MgCl_2$, 8 Na-gluconate, 3 KCl, 1 K2-EGTA, 4 K2-ATP, and 0.3 Na3-GTP at pH 7.25 with 10 HEPES. The solution also contained 50 µM Alexa 594 hydrazide (Thermo-Fisher) to visualise the morphology of the dendritic arbour. The example cell was dialysed with dye for 30 minutes before the patch electrode was slowly withdrawn prior to imaging. Images were post-processed in Fiji to subtract background using rolling ball radius, and enhance connectivity while removing speckles using the Gaussian Blur 3D filter and smooth functions.

3DMorph Workflow

The overall workflow of 3DMorph is outlined in Figure 1. Once images are acquired and processed as necessary, they should be moved to the Current Folder within Matlab, or the data folder should be added to Matlab's search path. The user first selects 'Interactive Mode' or 'Automatic Mode'. Any time a new batch of images with different threshold settings or xyz scales are being processed, it is necessary to run the program in Interactive Mode. The user inputs the file of interest, its xy and z scale, the number of channels included in the image, and the channel of interest (Figure 1A). Either .tiff or .lsm files are accepted. The user then adjusts threshold and size cut-off values (as discussed in detail below; Figure 1B-D). Finally, a folder is created to store figures, and an Excel file of results is saved (Figure 1E). Output values include data obtained prior to small object removal (average centroid distance between cells, total territorial volume, uncovered volume, percent covered volume), and from individual full cells (cell and territorial volumes, ramification index, number of endpoints and branch points, and average, minimum, and maximum branch lengths). If the user selects the option, a separate Excel file containing a list of all branch lengths can be generated for each cell. Once an Interactive Mode analysis is complete,

10

a parameter file will be created to save relevant input values. This can then be used to batch process a group of files using the same values and settings.

Threshold Images

Images saved as .lsm or .tiff files (Figure 2A) are opened using the bfopen, or imread functions, respectively. A threshold value, based on Otsu method (Otsu, 1979) is then set. A new window will appear (Figure 2B), showing the middle image of the z-stack, which can be used for a reference in deciding threshold values. A slider on the left sets the threshold level, and an automatically updated image shows the results of selected threshold values. The purpose of this step is to select a threshold level that accurately separates the small processes from background signal. Once an appropriate level is chosen, the 'Try this…' button passes the threshold adjustment value to the noise filter. Again, a slider on the left can be adjusted to decide the minimum size of objects that should be considered noise. This filter functions in 3D, so if a process is removed here, it was likely separated from the cell in the thresholding step. Small cells and processes will be excluded in a later step (Figure 2E), so it is not necessary to exclude them as noise here – they contribute to the calculation of total occupied brain volume. If selected, a threshold output image (Figure 2C) can be generated, which is a projection of the thresholded z-stack, where the thicker portions of cells (such as somas) are displayed in yellow and thinner portions are in blue. This colour coding is only used to visualize the approximate 3D shape of cells in a 2D image, and can be helpful to ensure the selected threshold value is correctly separating the cell from background signal.

Identify and Segment Cells

The resulting thresholded image is separated into objects based on their 3D connectivity. To segment erroneously connected cells, identify the largest cell that is not two cells connected (Figure 2D). Any

11

220 object above this threshold (Figure 2d', d'') is automatically segmented by fitting a Gaussian mixture
221 distribution (Matlab function fitgmdist) to the data (Figure 2d''').

222 Total Territorial Area of Microglia

223 As microglia are highly ramified cells, the volume of brain they survey is greater than the volume of the
224 cell itself. To estimate total territorial volume of microglia, a polygon is created to surround the outside
225 points of each cell, and its volume is measured. All small cells and processes from above or below the
226 image are included here. The amount of unoccupied volume and percentage of volume covered is also
227 determined.

228 Identify Full Cells

229 To get accurate volume and branching data of individual microglia, it is important to eliminate cells that
230 are partially excluded from the image. The user selects the smallest full cell (any smaller objects are
231 removed from further processing), and indicates whether cells touching the xy border should be
232 removed (Figure 2E). From the remaining cells (Figure 2F), cell volumes and territorial volumes (Figure
233 3A) are recorded. Cell volume is calculated by converting the number of voxels in each object to a real-
234 world unit based on the specified scaling factors. Cell ramification index (or extent) is calculated by
235 territorial volume divided by cell volume. This is a measure of how ramified or amoeboid the cells are.
236 For instance, a small ramified cell and a bushy cell may have a similar cell volume, but the bushy cell will
237 occupy more of its territorial space, therefore the ramification index measure will be smaller.

238 Distance Between Cell Centroids

239 Distribution of cells is addressed by measuring the average distance between centroids. Accurate
240 centroids (unbiased by the 'weight' of processes), are determined by eroding the cell to leave only the

12

soma. These coordinates are converted to the unit of interest by multiplying the specified scales, and the distance between them is calculated. The average centroid distance is saved to the final results file.

3D Skeletonization and Branch Tracing

To calculate branch lengths, endpoints, and branch points, a 3D skeleton of each cell is first generated. In 3DMorph, two skeletonization methods are available (Figure 3B). The first keeps all small processes (Figure 3D). This is ideal for images taken at a high magnification or to investigate differences in small filipodia-like structures. However, this method is also much slower and computationally demanding. This method is accomplished using the Skeleton3D method, developed by Kerschnitzki and colleagues (Kerschnitzki et al., 2013), and is available on File Exchange (https://www.mathworks.com/matlabcentral/fileexchange/43400-skeleton3d). Small extensions remaining on the skeleton, which are not likely to be true processes, are removed using the Graph2Skel3D and Skel2Graph3D (available at https://www.mathworks.com/matlabcentral/fileexchange/43527-skel2graph-3d).

The second skeleton method looks only at large branches and ignores smaller structures (Figure 3E). This method might be preferred in images with a lower magnification and with several cells per image. It processes the skeleton using the Accurate Fast Marching method (made available by authors at https://www.mathworks.com/matlabcentral/fileexchange/24531-accurate-fast-marching).

Within each skeleton, endpoints are identified as pixels attached to only one other pixel. For each endpoint, a path between the endpoint and the centroid of the cell is traced to create a mask of each branch, from which the length is measured. This method may give a longer average branch length than other methods, as each end is traced to the soma, rather than to the nearest branch point. However, this method is more sensitive to differences in highly ramified vs bushy or amoeboid cells.

13

By adding the masks of all branches, a colour code is generated with primary branches in red as those that have been traced 4 or more times, secondary branches in yellow have been traced 3 times, tertiary in green have been traced twice, and quaternary in blue have been traced only once (most distal process, which terminate in an endpoint). From this process mask, the number of branch points are calculated by determining points of intersection between primary, secondary, tertiary, or quaternary branches.

If requested, a new folder is generated in the Current Folder titled as '*filename*_figures' to save specified images and branch lengths. 3D representations of original cells (Figure 3C), endpoints, branch points, and skeletons (Figure 3D, E) can be saved. Images of initial thresholding, identified objects, segmented objects, and full cells will also be saved to this folder if the user chooses to have them generated.

Export Data

Finally, the data is written to an Excel file titled 'Results*filename*' and saved to Matlab's Current Folder. For each image, the exported data includes: average centroid distances, total microglial territory volume, total unoccupied volume, and percentage of volume occupied. For each full cell: territory volume, cell volume, ramification index, number of endpoints and branch points, and average, minimum, and maximum branch lengths are saved.

Statistics

All data was analyzed using a one-way ANOVA with a significance level of $p < 0.05$.

14

Results

Accuracy of 3DMorph Results

To validate our 3DMorph program, we generated a test image to process and compare with current analysis methods (Figure 4A, B). The image size is 512 x 512 pixels with 100 slices (0.21 µm/pixel, and 1 µm/slice). We analyzed this image in 3DMorph (Figure 4C, D, E), as well as with the 3D-tracing ImageJ plugin, Simple Neurite Tracer (Figure 4F), and by freehand tracing of a maximum intensity z-projection image (Figure 4G). Features of each method are summarized in Table 1.

When comparing these techniques, there was no significant difference in the number of endpoints or branch points identified (Figure 4H, I). However, process overlap in z-projected images led to greater uncertainty in separating branches of individual cells. Cell volumes were similar between 3DMorph and Simple Neurite Tracer (Figure 4J), but are unavailable from z-projected data.

Maximum and average branch lengths were significantly greater when processed by 3DMorph compared to z-projected images (Figure 4K, L), confirming the importance of maintaining 3D information. While Simple Neurite Tracer does analyze length in 3D, we found that these values are lower than our 3DMorph analysis. This is likely because 3DMorph measures the length of each endpoint to the soma centroid instead of the distance between an endpoint and its parent branch.

Processing Time of 3DMorph

In addition to providing similar or more accurate measurements, 3DMorph also took considerably less time for the same investigator to complete the analysis of the test image (1 min, 12 s) compared to Simple Neurite Tracer (59 min, 3 s) or z-projection tracing (23 min, 35 s) (Figure 4M). While times were measured using Interactive Mode processing on one image, 3DMorph's Automatic Mode processing would be even more advantageous.

15

Finally, while both Simple Neurite Tracer and z-projections require subjective branch tracing, 3DMorph completes these steps automatically. Therefore, variability between researchers will be greatly decreased, while improving data reproducibility among researchers and between labs.

Microglial Morphology Changes in Response to Local Cues

We next used 3DMorph to compare conditions which cause or mimic an increase or decrease in neuronal activity. As previously published (Dissing-Olesen et al., 2014), application of ATP triggers microglial process outgrowth, whereas processes retract in the presence of CNQX and TTX (Fontainhas et al., 2011). While the biological pathways leading to these changes are interesting, here we do not address the biological cause of the process extensions or retractions. Instead we use these pharmacological manipulations only as tools to alter microglial morphology.

Acute hippocampal slices from CX3CR1$^{EGFP/+}$ mice were incubated with either control aCSF (Figure 5 A, B), 500 µM ATP (Figure 5 C, D), or 50 µM CNQX with 1 µM TTX (Figure 5 E, F) at 32 °C. Slices were fixed using the SNAPSHOT protocol (Dissing-Olesen & MacVicar, 2015) and imaged by 2-photon microscopy. A 1024 x 1024 image with 50 z-slices was acquired (xy scale: 0.17 µm/pixel; z scale: 1 µm/slice; image dimensions are 174.08 x 174.08 x 50 µm). The same parameter file was used to automatically process images from these three conditions, removing any risk of experimenter bias.

3DMorph analysis revealed a significant increase in the percentage of brain volume surveyed by microglia in ATP conditions, whereas CNQX/TTX treatment decreased relative to control (Figure 5G). When single cells were analyzed, the territorial volume of each cell treated with CNQX/TTX was significantly smaller than in control aCSF (Figure 5H), while ATP induced a small increase. Finally, 3DMorph quantification confirmed that there is a significant increase in branch length of ATP-treated microglia, while CNQX/TTX-treated microglia have significantly shorter branches (Figure 5I). These

16

results demonstrate the ability of 3DMorph to automatically quantify morphological changes of microglia *in situ* across different conditions in an automatic, unbiased, and reproducible manner.

Microglial Morphology *in vivo*

While *in situ* imaging has many advantages, there is a growing push in the scientific field to confirm results using *in vivo* experiments. As 3DMorph requires only one channel containing the microglia image, and does not rely on counterstaining, it is possible to process microglia images from *in vivo* data.

We confirm this by processing microglia images of CX3CR1$^{EGFP/EGFP}$ mice acquired through a cranial window on an *in vivo* 2-photon microscope (Figure 6A). Image stacks were taken at 512 x 512 with 40 slices at an interval distance of 1 µm. 3DMorph analysis accurately thresholded (Figure 6B), segmented (Figure 6C), and skeletonized (Figure 6D-G) these images, confirming that 3DMorph is appropriate for analyzing *in vivo* microglial morphology.

Morphology of Neurons

A benefit of 3DMorph's Interactive Mode is that the software is adaptable to work with many types of input data. This makes it possible to process other types of branched cells in addition to microglia, such as neurons, astrocytes, or oligodendrocyte precursor cells. We validate 3DMorph's performance in processing a patched and dye-loaded neuron (Figure 7A). 3DMorph accurately identifies and maintains only the neuron (Figure 7B), and skeletonizes the processes (Figure 7C). Given the size difference between microglia and neurons, we therefore validate that 3DMorph correctly processes images of branched cells other than microglia.

17

Discussion

Here, we present a novel method that allows for rapid and unbiased analysis of microglial morphologies in 3 dimensions. This is an open source script running in Matlab, which is widely available through academic institutions, making 3DMorph free and easily accessible. We have written the program to make it user-friendly and compatible with many imaging settings. Furthermore, the program is well suited for analysis of other branched cells, such as astrocytes or oligodendrocyte precursor cells, in addition to microglia and neurons.

This program is an advancement to the currently available methods, as it relies on minimal user input, making it fast, replicable between experimenters and labs, and not subject to bias. Once parameters have been chosen, Automatic Mode processes large amounts of data with minimal input time. Importantly, using 3DMorph maintains the 3D information of cells, providing more accurate volume and branch length measurements.

We have validated 3DMorph against two other analysis techniques (Simple Neurite Tracer, and z-projection tracing), and detected alterations in microglial morphology e.g. hyper-ramification triggered by ATP and hypo-ramification triggered by CNQX. Importantly, 3DMorph is compatible with images obtained *in vivo* and images of other branching cell types.

Another automatic 3D microglial analysis program has recently been published (Heindl et al., 2018). While this is a powerful program offering a range of output results, our 3DMorph program offers some key advantages. Most importantly, it does not require a DAPI input image, which removes the necessity for immunostaining and makes 3DMorph capable of handling *in vivo* data. Furthermore, 3DMorph can process .tiff files, which allows the processing of images acquired by multiple types of software. We have also shown here that 3DMorph can manage thick sections of tissue and reliably separate cells that may appear overlapped when z projected. Finally, although a completely automated analysis is available

18

in 3DMorph, we first implement a series of graphical user interfaces that show real-time updates of how chosen settings will process the data. This transparency allows the user to confirm that the program is correctly processing their data.

Another promising analysis tool, ProMoIJ (Paris, 2018), has been recently published, which looks at microglial process motility. While this method is excellent at analyzing tip extension and retraction, it does not analyze morphology differences of whole-cell images. Microglial morphology provides a clue to the cell's biological function. Therefore, shape measurements (ie. branch length and estimations of extent) are often used to differentiate healthy microglia from those associated with disease (Baron et al., 2014; Doorn et al., 2014; Kreutzberg, 1996; Perego et al., 2013; Torres-Platas et al., 2014). We encourage the field to use our 3DMorph program to perform their morphological quantifications, and we gladly supply the original code ([https://github.com/ElisaYork/3DMorph]) so that it can be adapted and improved upon by labs to best meet their needs.

Troubleshooting

While we have tried to make this program robust, user-friendly, and adaptable, it is possible issues may still occur. We have compiled this list of possible errors to assist with troubleshooting.

Errors When Running the Script

1. Mex file error, or all output data for full cells is "0":

   At the skeletonization step, if the script encounters an error, it will output zeros for this cell and move on to the next cell in the file. If all cells encountered an error, it is likely a mex compiling issue. Some skeletonization functions need to be compiled from C to Matlab. In the original folder, go to: Functions>FastMarching_version3b>compile_c_files. You will need a compatible compiler to run this. If you do not have one, Matlab will provide instructions on installing one.

19

2. ThresholdGUI:

   If you would like to keep the threshold and noise levels set to 0, please increase them, then move them back to 0. Be sure to confirm your adjusted values by pressing the 'Try This' and 'Update' buttons.

3. numObjMg = numel(FullMg):

   If you only have one cell in your image, you must choose to keep it during small cell removal by selecting the "Keep all cells" option. If this is not selected, your cell will be removed and pass on a blank image to the next processing step.

4. "waitbar" error:

   The program automatically generates waitbars to update you on how long it will take to process each step. It may reach an error if you have closed the waitbar window before it is finished processing.

5. GMModel: nuc must be a positive integer:

   During segmentation, the program erodes the connected cells to find nuclei and determine how many cells the object should be segmented into. If cells or nuclei are small (as in low magnifications), they may be eroded completely and a blank image will be passed on. In the first for loop of the Cell Segmentation portion of the script, decrease the value of se=strel('diamond',**4**); This will decrease the amount of erosion.

Unsatisfactory Data Processing

1. 3DMorph works best on images with high signal to noise ratio. During the image acquisition stage, try using a high magnification of the cells you would like to analyze and decrease the z-slice interval so that branches remain connected in this dimension. If available, deconvolution

post-processing may be helpful. It may also help to remove background before processing. This can be done with Fiji's rolling ball radius subtraction.

2. If there is too much connectivity, the program will have trouble segmenting properly. Try increasing the threshold level so that fewer branches remain touching in the binary image.
3. If you observe too much connectivity that can not be fixed by increasing threshold levels, try using a spatial sampling of 0.166 µm/pixel, for example a 1024x1024 pixel image with a size of 170x170 µm. Your input images can be scaled in ImageJ prior to analysis to match this pixel density. See ImageJ, Image menu scale function.
4. When batch processing images, it is beneficial to spend time finding parameters that work well for all files. Test a few example images in Interactive Mode to determine which settings are best. To save time, you can run the program until you have chosen a threshold, and large and small cell limit, then exit before it begins measuring skeletons. Once you have chosen suitable parameters, you will need to let the program run fully to generate a Parameters output file to use in your batch processing.
5. For accurate total image coverage, keep a low noise level so that small processes are still included. Small cells and processes from out-of-frame cells can be removed at a later step.

References:

Baron, R., Babcock, A. A., Nemirovsky, A., Finsen, B., & Monsonego, A. (2014). Accelerated microglial pathology is associated with Abeta plaques in mouse models of Alzheimer's disease. *Aging Cell*, *13*(4), 584–595. https://doi.org/10.1111/acel.12210

Davalos, D., Grutzendler, J., Yang, G., Kim, J. V., Zuo, Y., Jung, S., … Gan, W. B. (2005). ATP mediates rapid microglial response to local brain injury in vivo. *Nature Neuroscience*, *8*(6), 752–758.

21

437 https://doi.org/10.1038/nn1472

438 Davis, E. J., Foster, T. D., & Thomas, W. E. (1994). Cellular forms and functions of brain microglia. *Brain*

439 *Research Bulletin*, *34*(1), 73–78. https://doi.org/10.1016/0361-9230(94)90189-9

440 Dissing-Olesen, L., LeDue, J. M., Rungta, R. L., Hefendehl, J. K., Choi, H. B., & MacVicar, B. a. (2014).

441 Activation of Neuronal NMDA Receptors Triggers Transient ATP-Mediated Microglial Process

442 Outgrowth. *Journal of Neuroscience*, *34*(32), 10511–10527.

443 https://doi.org/10.1523/JNEUROSCI.0405-14.2014

444 Dissing-Olesen, L., & MacVicar, B. A. (2015). Fixation and Immunolabeling of Brain Slices: SNAPSHOT

445 Method. *Current Protocols in Neuroscience*, *71*(1), 1.23.1-1.23.12.

446 https://doi.org/10.1002/0471142301.ns0123s71

447 Doorn, K. J., Goudriaan, A., Blits-Huizinga, C., Bol, J. G. J. M., Rozemuller, A. J., Hoogland, P. V. J. M., …

448 Van Dam, A. M. (2014). Increased amoeboid microglial density in the Olfactory Bulb of Parkinson's

449 and Alzheimer's Patients. *Brain Pathology*, *24*(2), 152–165. https://doi.org/10.1111/bpa.12088

450 Drew, P. J., Shih, A. Y., Driscoll, J. D., Knutsen, P. M., Blinder, P., Davalos, D., … Kleinfeld, D. (2010).

451 Chronic optical access through a polished and reinforced thinned skull_supp. *Nature Methods*,

452 *7*(12), 981–4. https://doi.org/10.1038/nmeth.1530

453 Erny, D., Hrabě de Angelis, A. L., Jaitin, D., Wieghofer, P., Staszewski, O., David, E., … Prinz, M. (2015).

454 Host microbiota constantly control maturation and function of microglia in the CNS. *Nature*

455 *Neuroscience*, *18*(7). https://doi.org/10.1038/nn.4030

456 Eyo, U. B., Gu, N., De, S., Dong, H., Richardson, J. R., & Wu, L.-J. (2015). Modulation of Microglial Process

457 Convergence Toward Neuronal Dendrites by Extracellular Calcium. *Journal of Neuroscience*, *35*(6),

458 2417–2422. https://doi.org/10.1523/JNEUROSCI.3279-14.2015

459 Eyo, U. B., Peng, J., Swiatkowski, P., Mukherjee, A., Bispo, A., & Wu, L.-J. (2014). Neuronal Hyperactivity

460 Recruits Microglial Processes via Neuronal NMDA Receptors and Microglial P2Y12 Receptors after

461 Status Epilepticus. *Journal of Neuroscience*, *34*(32), 10528–10540.
462 https://doi.org/10.1523/JNEUROSCI.0416-14.2014
463 Fontainhas, A. M., Wang, M., Liang, K. J., Chen, S., Mettu, P., Damani, M., … Wong, W. T. (2011).
464 Microglial morphology and dynamic behavior is regulated by ionotropic glutamatergic and
465 GABAergic neurotransmission. *PLoS ONE*, *6*(1). https://doi.org/10.1371/journal.pone.0015973
466 Hefendehl, J. K., Neher, J. J., Suhs, R. B., Kohsaka, S., Skodras, A., & Jucker, M. (2014). Homeostatic and
467 injury-induced microglia behavior in the aging brain. *Aging Cell*, *13*(1), 60–69.
468 https://doi.org/10.1111/acel.12149
469 Heindl, S., Gesierich, B., Benakis, C., Llovera-Garcia, G., Duering, M., & Liesz, A. (2018). Automated
470 Morphological Analysis of Microglia After Stroke. *Frontiers in Cellular Neuroscience*, *12*(April), 106.
471 https://doi.org/10.3389/FNCEL.2018.00106
472 Hines, D. J., Hines, R. M., Mulligan, S. J., & Macvicar, B. A. (2009). Microglia processes block the spread of
473 damage in the brain and require functional chloride channels. *Glia*, *57*(15), 1610–1618.
474 https://doi.org/10.1002/glia.20874
475 Jung, S., Aliberti, J., Graemmel, P., Sunshine, M. J., Kreutzberg, G. W., Sher, A., & Littman, D. R. (2000).
476 Analysis of fractalkine receptor CX(3)CR1 function by targeted deletion and green fluorescent
477 protein reporter gene insertion. *Mol Cell Biol*, *20*(11), 4106–4114. Retrieved from
478 http://www.ncbi.nlm.nih.gov/pubmed/10805752
479 Karperien, A., Ahammer, H., & Jelinek, H. F. (2013). Quantitating the subtleties of microglial morphology
480 with fractal analysis. *Frontiers in Cellular Neuroscience*, *7*(January), 1–18.
481 https://doi.org/10.3389/fncel.2013.00003
482 Kerschnitzki, M., Kollmannsberger, P., Burghammer, M., Duda, G. N., Weinkamer, R., Wagermaier, W., &
483 Fratzl, P. (2013). Architecture of the osteocyte network correlates with bone material quality.
484 *Journal of Bone and Mineral Research*, *28*(8), 1837–1845. https://doi.org/10.1002/jbmr.1927

485 Kloss, C. U. A., Bohatschek, M., Kreutzberg, G. W., & Raivich, G. (2001). Effect of lipopolysaccharide on
486 the morphology and integrin immunoreactivity of ramified microglia in the mouse brain and in cell
487 culture. *Experimental Neurology*, *168*(1), 32–46. https://doi.org/10.1006/exnr.2000.7575
488 Kozlowski, C., & Weimer, R. M. (2012). An automated method to quantify microglia morphology and
489 application to monitor activation state longitudinally in vivo. *PLoS ONE*, *7*(2), 1–9.
490 https://doi.org/10.1371/journal.pone.0031814
491 Kreutzberg, G. W. (1996). Microglia: A sensor for pathological events in the CNS. *Trends in*
492 *Neurosciences*, *19*(8), 312–318. https://doi.org/10.1016/0166-2236(96)10049-7
493 Lou, N., Takano, T., Pei, Y., Xavier, A. L., Goldman, S. A., & Nedergaard, M. (2016). Purinergic receptor
494 P2RY12-dependent microglial closure of the injured blood–brain barrier. *Proceedings of the*
495 *National Academy of Sciences*, *113*(4), 1074–1079. https://doi.org/10.1073/pnas.1520398113
496 Nimmerjahn, A., Kirchhoff, F., & Helmchen, F. (2005). Resting Microglial Cells Are Highly Dynamic
497 Surveillants of Brain Parenchyma in Vivo, *308*(May), 1314–1319.
498 https://doi.org/10.1126/science.1110647
499 Otsu, N. (1979). A threshold selection method from gray-level histograms. *IEEE Transactions on Systems,*
500 *Man, and Cybernetics*, *9*(1), 62–66. https://doi.org/10.1109/TSMC.1979.4310076
501 Paris, I. (2018). ProMoIJ : a new tool for automatic three-dimensional analysis of microglial processes
502 motility.
503 Perego, C., Fumagalli, S., & De Simoni, M.-G. (2013). Three-dimensional Confocal Analysis of
504 Microglia/macrophage Markers of Polarization in Experimental Brain Injury. *Journal of Visualized*
505 *Experiments*, (79), 1–7. https://doi.org/10.3791/50605
506 Rosenegger, D. G., Tran, C. H. T., LeDue, J., Zhou, N., & Gordon, G. R. (2014). A high performance, cost-
507 effective, open-source microscope for scanning two-photon microscopy that is modular and readily
508 adaptable. *PLoS ONE*, *9*(10). https://doi.org/10.1371/journal.pone.0110475

509 Takayama, F., Hayashi, Y., Wu, Z., Liu, Y., & Nakanishi, H. (2016). Diurnal dynamic behavior of microglia
510 in response to infected bacteria through the UDP-P2Y 6 receptor system. *Scientific Reports*, *6*(July),
511 1–10. https://doi.org/10.1038/srep30006
512 Torres-Platas, S. G., Comeau, S., Rachalski, A., Bo, G. D., Cruceanu, C., Turecki, G., … Mechawar, N.
513 (2014). Morphometric characterization of microglial phenotypes in human cerebral cortex. *Journal*
514 *of Neuroinflammation*, *11*. https://doi.org/10.1186/1742-2094-11-12
515 Verdonk, F., Roux, P., Flamant, P., Fiette, L., Bozza, F. A., Simard, S., … Danckaert, A. (2016). Phenotypic
516 clustering: A novel method for microglial morphology analysis. *Journal of Neuroinflammation*,
517 *13*(1). https://doi.org/10.1186/s12974-016-0614-7
518

Table Legend

3DMorph, Simple Neurite Tracer ImageJ plugin, and freehand tracing of maximum z-projection images. While both 3DMorph and Simple Neurite Tracer process 3D information, only 3DMorph offers an automatic batch processing mode to greatly decrease user input time.

Figure Legends

Figure 1: 3DMorph workflow.

The user selects either Interactive or Automatic mode. Interactive mode must be used first to generate a parameters file. (A) The user then selects the file to analyze, and specifies xy and z scale, number of channels, and the channel of interest. Both .tiff and .lsm files are supported. The original image (B) is loaded and 3D connected components (C) are automatically detected. (D) Large cells can be selected for segmentation and small objects can be removed. (E) After skeletonization and measurements of remaining cells, 3DMorph saves selected images and generates an Excel results file. Gray text indicates automatic steps.

Figure 2: Select threshold and identify cells.

(A) Grayscale maximum projection of original stack. Scale bar = 25 µm. (B) Select threshold level, and noise filter value to remove small spots. (C) 'Output Threshold Image' is a 2D projection after threshold and noise filters are applied. To visualize 3D shapes of cells, hotter colours indicate thicker portions of cells. (D) 3DMorph automatically identifies 3D connected components, and the user selects a maximum cell size. Objects larger than this value are considered to be erroneously connected cells (d', d''), and will

26

be segmented into separate objects (d'''). (E) Exclude remaining small cells, out-of-focus processes, or cells touching the xy borders to isolate only full cells (F). (G) At this point, the program records total occupied volume (calculated before excluding small cells, processes, etc.), the unoccupied volume, and the distance between cell centroids.

Figure 3: Analysis of individual full cells.

(A) Territorial volume of each cell is determined by placing a polygon around all of the extreme points of the cell. (B) The user decides which skeletonization method to use and which images to save (including: original cell, skeleton, branch points, and end points). Each full cell (C) is then processed individually to generate a 3D skeleton, keeping either all branches (D), or only major branches (E). In skeleton figures, colors indicate order of connectivity (red = primary, yellow = secondary, green = tertiary, and blue = connected to endpoint). (F) After processing all cells, the program outputs territorial volume, cell volume, ramification index (calculated as territorial volume / cell volume), number of endpoints and branch points, as well as average, maximum, and minimum branch length for each cell. A complete list of branch lengths for each cell can also be generated.

Figure 4: Validation and comparison of 3DMorph with current analysis tools.

(A) 3D visualization of a manually-generated test image composed of four cells with overlapping processes. (B) Z-projection of test image. Scale bar = 25 µm. (C) Full cells as identified by 3DMorph. (D) A single full cell from the test image (outlined by dashed box in C). (E) 3D skeleton generated automatically by 3DMorph. (F) 3D skeleton manually drawn using Simple Neurite Tracer (SNT). (G) 2D skeleton manually drawn using freehand tracing of a z-projection of the test image. Based on analysis by

27

562 3DMorph, SNT, or z-projection tracing, there is no significant difference in the number of endpoints (H)
563 or branch points (I) recorded. (J) Cell volume measurements are accurate between 3DMorph and SNT,
564 but unavailable from z-projection analysis. (K) Maximum branch length is significantly longer by
565 3DMorph and SNT analysis than by z-projection tracing. (L) Average branch lengths are significantly
566 longer by 3DMorph than by SNT or z-projection. (M) Comparison of user input time to measure data.
567 Error bars indicate mean +/- SEM. *p<0.05, **p<0.01, ***p<0.001 by one-way ANOVA.

568

569 ## Figure 5: Microglia morphology changes in response to local cues.

570 Microglia are incubated with control aCSF (A, B), 500 µM ATP (C, D), or 50 µM CNQX and 1 µM TTX (E, F)
571 before fixing and imaging (imaging dimensions: 174.08 x 174.08 x 50 µm). Original 3D projections (A, C,
572 E; scale bar = 25 µm), and remaining full cells (B, D, F), are shown. (G) Quantification confirms that
573 microglia cover more volume in ATP than in control conditions, while CNQX/TTX treatment decreases
574 the total surveyed volume. When only full cells are considered, each microglial cell in CNQX/TTX
575 conditions covers a smaller territorial volume (H) and has shorter average branch lengths (I) than control
576 or ATP conditions, while ATP cells have significantly longer branch lengths than control. Error bars
577 represent mean +/- SEM. *p<0.05, **p<0.01, ***p<0.001, ****p<0.0001 by one-way ANOVA.

578

579 ## Figure 6: Morphology analysis of in vivo microglia images.

580 A) Maximum projection of *in vivo* image stack. B) 3DMorph threshold image shown as a maximum
581 projection. C) Separation of thresholded image into individual objects, colour-coded based on size of
582 object. D) Remaining full cells after removing small processes from out-of-frame cells. E) Isolated single
583 cell from outlined region in D. F) Skeleton of major branches and G) skeleton maintaining fine processes.

28

584

585 Figure 7: Morphology analysis of dye-loaded neuron.

586 A) Maximum projection of dye-loaded neuron; scale bar = 50 µm. B) Remaining cell following 3DMorph

587 thresholding. C) Skeletonized neuron keeping fine processes.

29

A

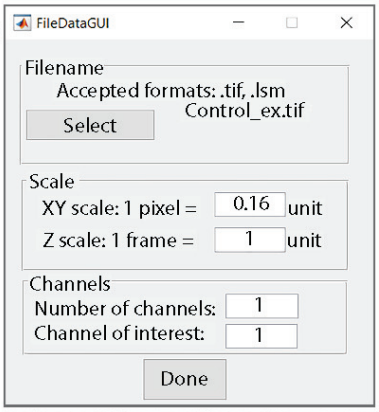

B

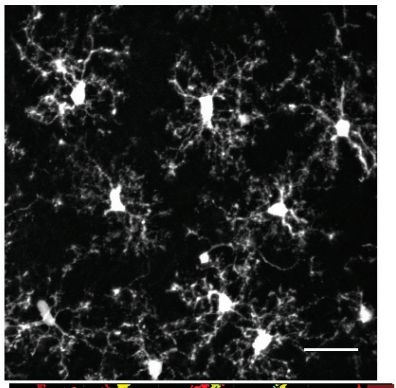

C

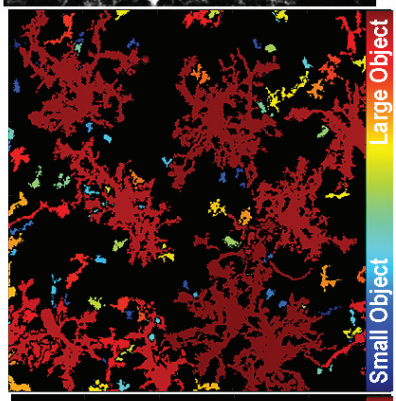

D

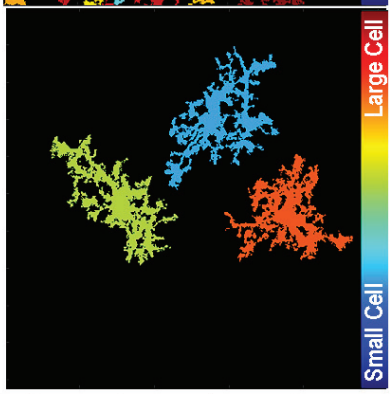

E

	A	B	C	D	E
1		ExCell_3Dblur-max		CellTerrito	46171.57
2	Avg Centrc	65.47897			72431.24
3	TotMgTerr	219124.6			55069.97
4	TotUnoccu	936930.5			45451.77
5	PercentOc	18.95451			

Choose Program Mode

`Interactive Mode':
Select image to analyze.
Set xy and z scaling factors.
Select channel of interest.

`Automatic Mode':
Choose parameters and images to batch process.

Run.

Retrieve results.

Adjust threshold level.
Remove noise.

Detect object connectivity in 3D.
Separate data into objects.

Select the maximum cell size
(larger objects are segmented).
Select the minimum cell size
(smaller objects are removed).

In only remaining full cells:
Skeletonize
Trace branches
Identify branch points
and endpoints.

Save figures.
Output results.

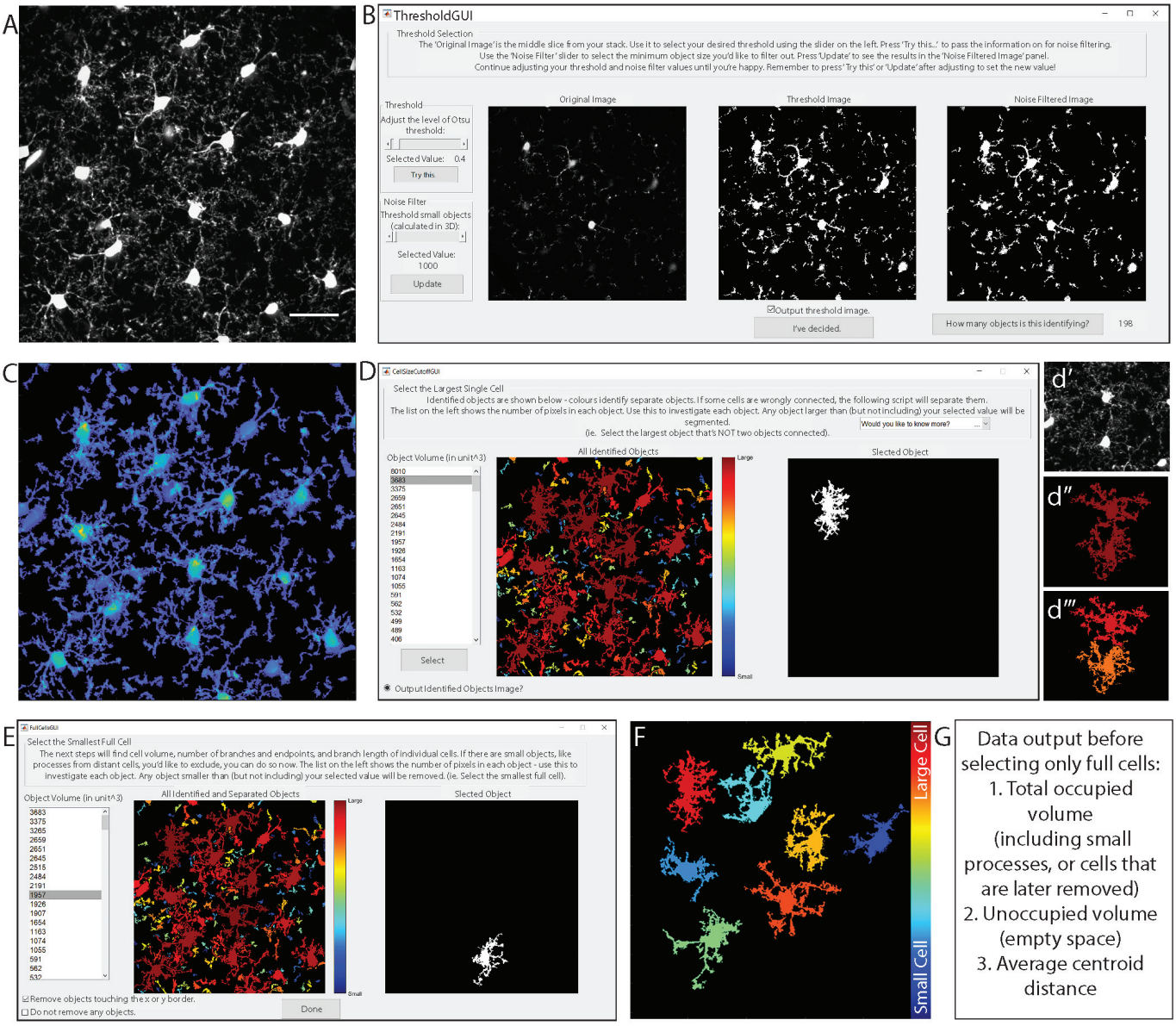

A

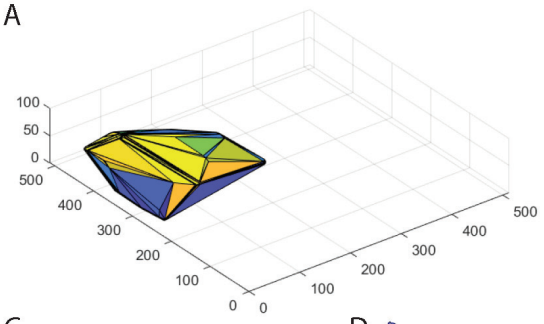

B

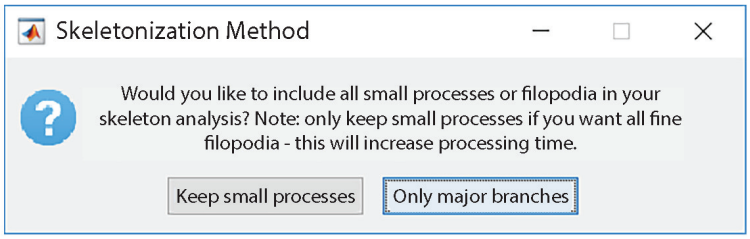

C

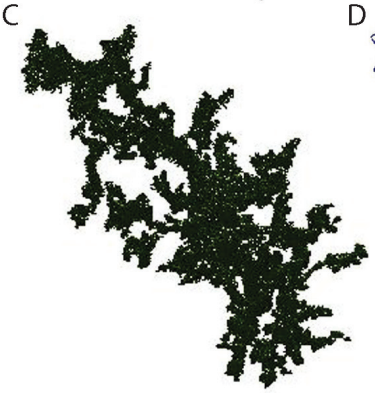

D

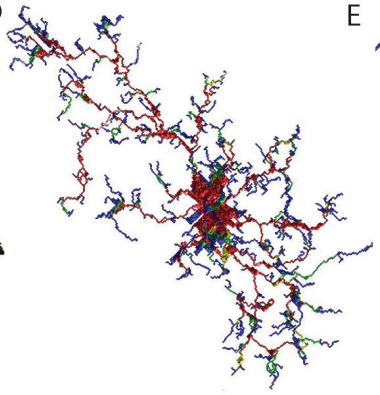

E

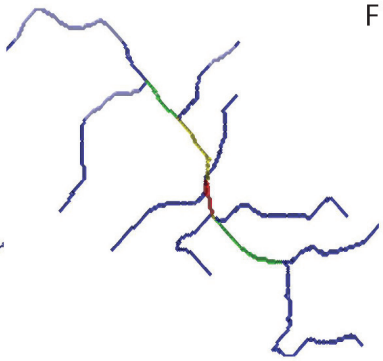

F

Data from each cell:
1. Territorial volume
2. Cell volume
3. Ramification index
4. Number of endpoints
5. Number of branch points
6. Average branch length
7. Max branch length
8. Min branch length
9. Branch length list

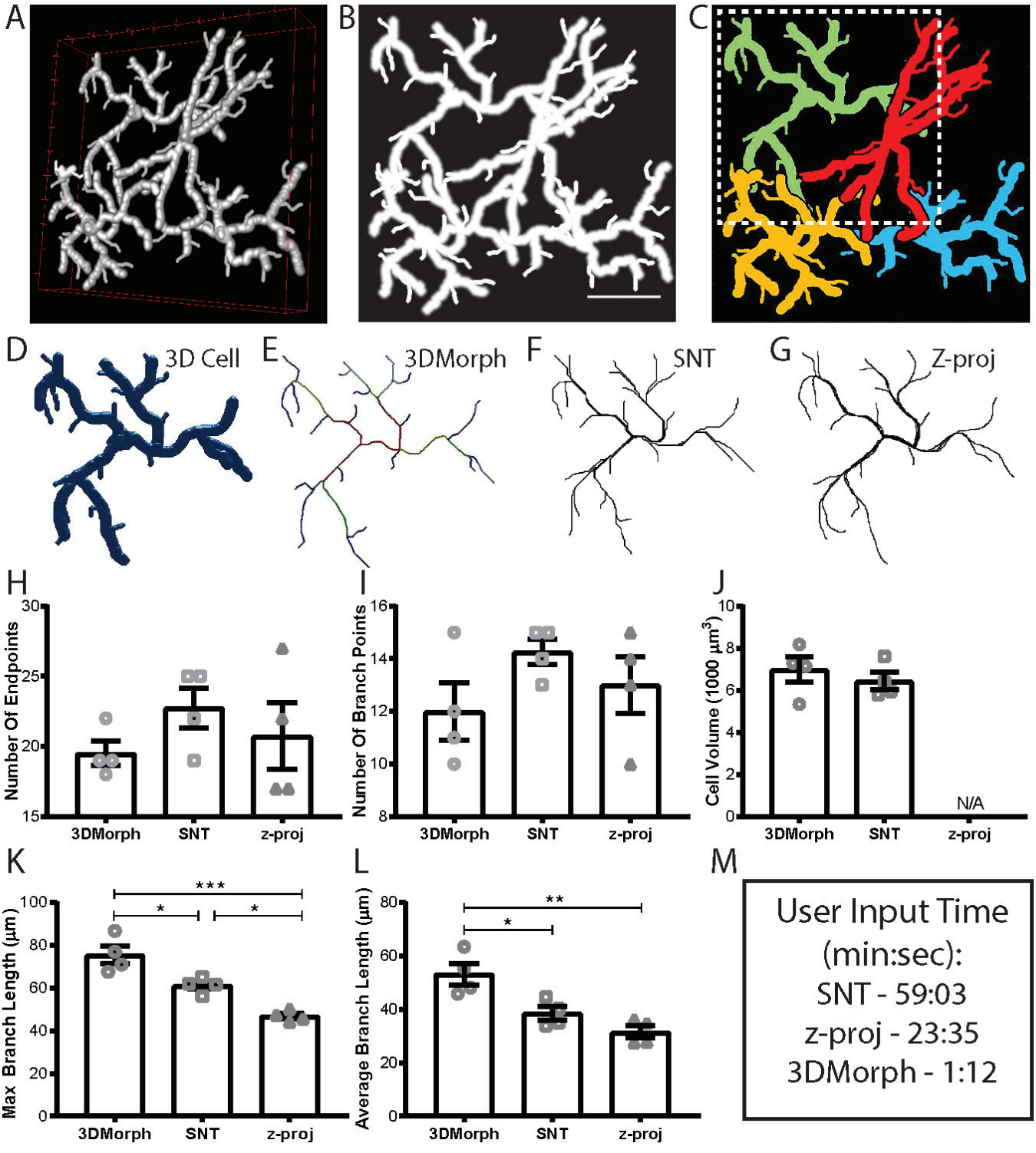

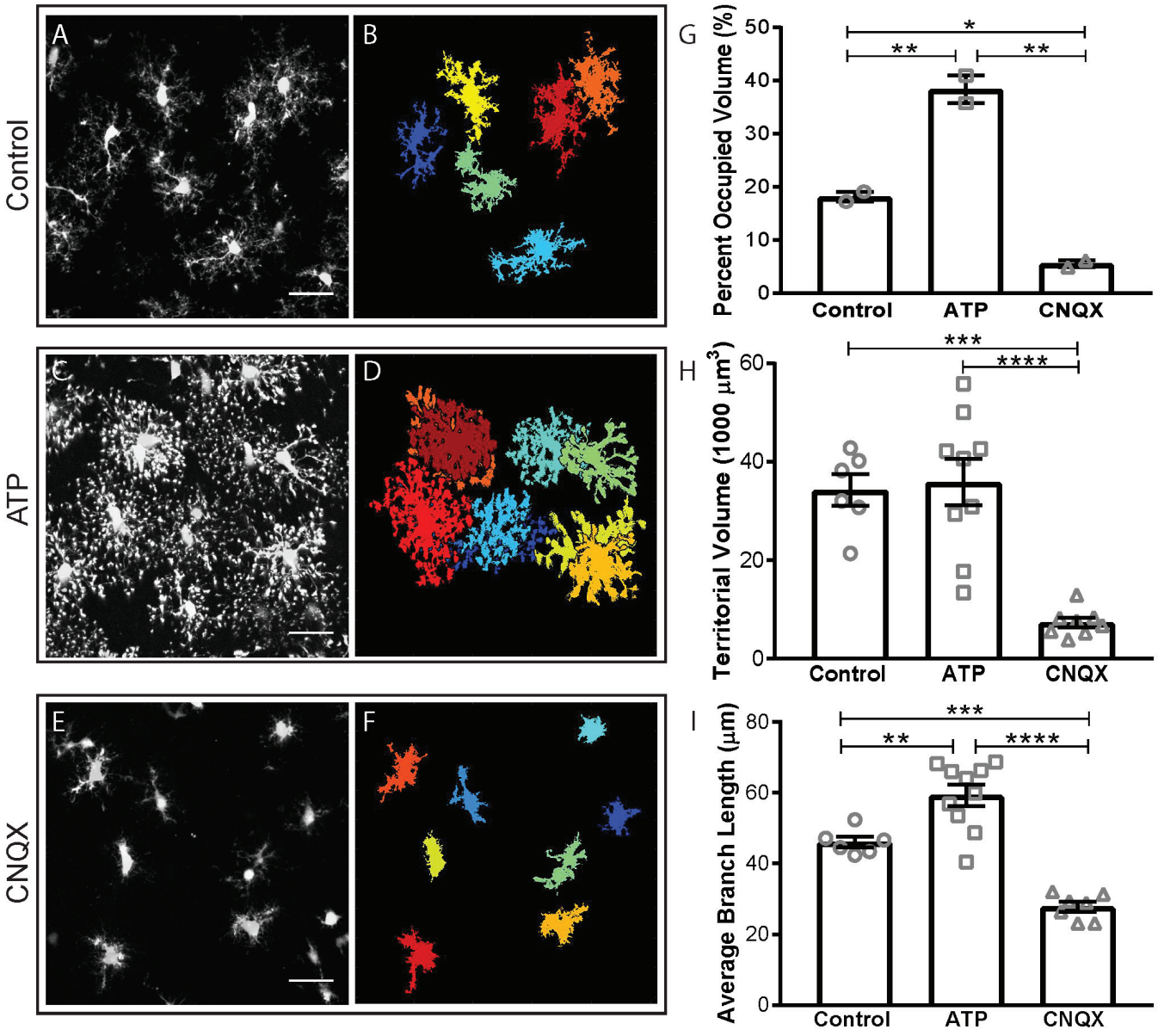

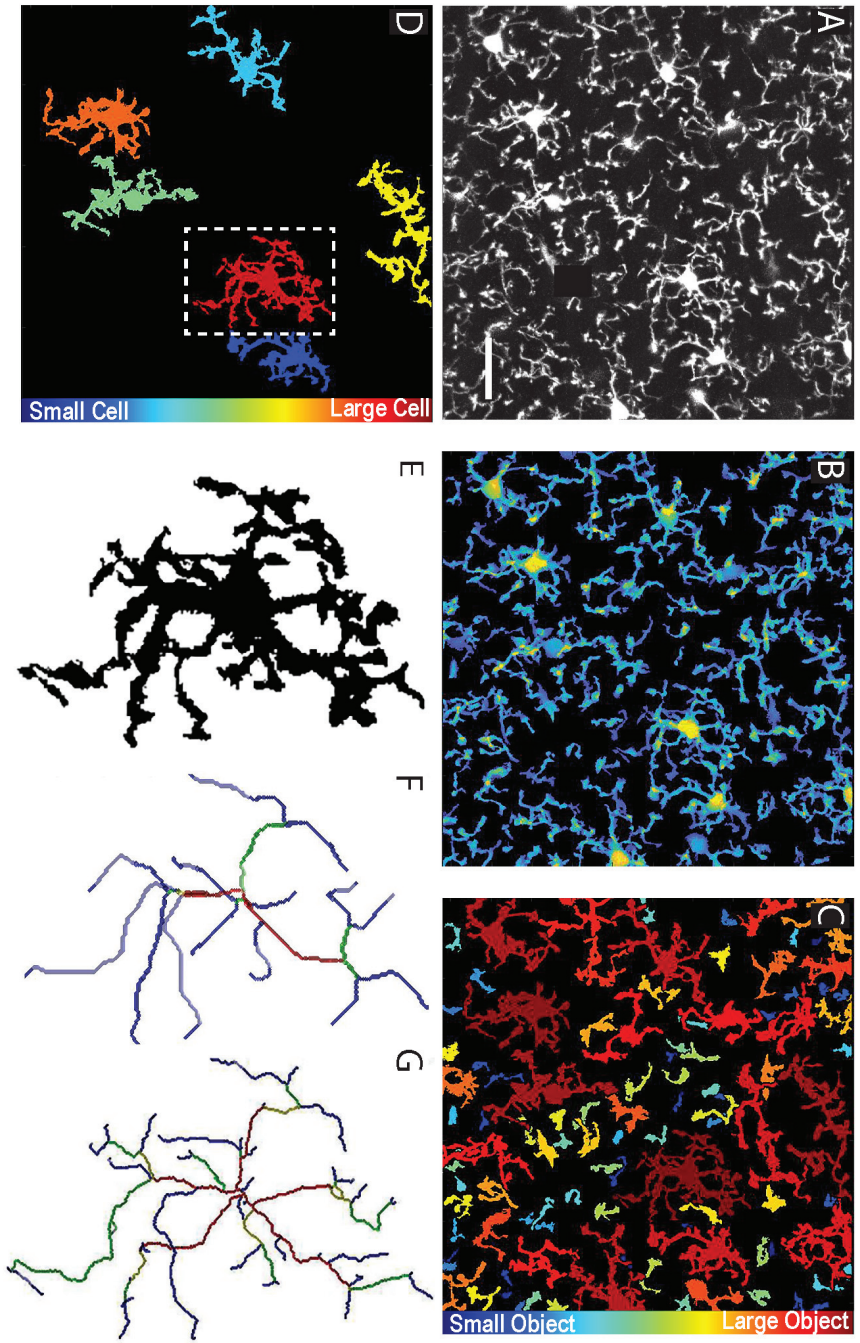

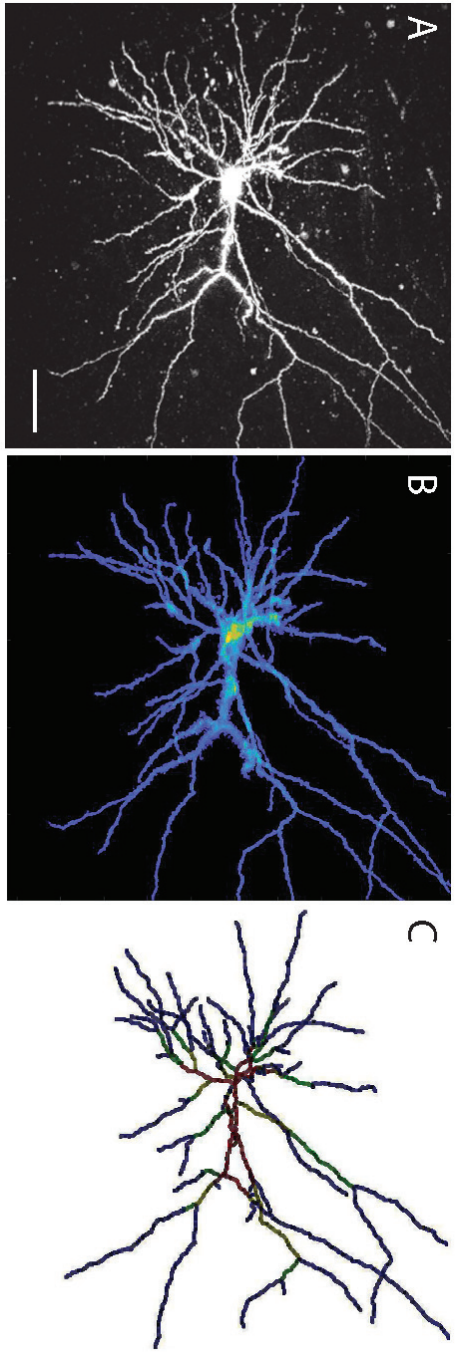

Table

	3DMorph	Simple Neurite Tracer	Z-Projection Trace
Branch Length	✓	✓	✓
Cell Volume	✓	✓	✗
Territorial Volume	✓	✗	✗
Total Occupied Volume	✓	✗	✗
Ramification Index	✓	✗	✗
# of Endpoints	✓	✓	✓
# of Branch Points	✓	✓	✓
3D Analysis	✓	✓	✗
Automatic Batch Processing	✓	✗	✗
User Input Time	Fastest (min)	Slowest (min-hr)	Intermediate (10s of min)